Dynamics of Ligand Escape in Myoglobin: Q-Band Transient Absorption and Four-Wave Mixing Studies

Jennifer P. Ogilvie,[‡] Marie Plazanet,[‡] Gami Dadusc,[†] and R. J. Dwayne Miller*[,‡]

Departments of Physics and Chemistry, University of Toronto, 80 St. George St., Toronto, Ontario M5S 3H6, Canada and Department of Physics, University of Rochester, Rochester, New York 14627

Received: December 10, 2001; In Final Form: June 27, 2002

The dynamics of ligand escape from carboxymyoglobin are studied via Q-band transient absorption and diffractive optics-based four-wave mixing. The latter approach provides an interferometric method for following protein motions and energetics and allows unambiguous assignment of different signal components to specific dynamical processes, a problem that has hindered all photothermal, photoacoustic, and grating methods in the past. In particular, the real part of the four-wave mixing signal is isolated, and it is demonstrated that the excited-state population contribution to the signal can be identified and removed by tuning the probe to wavelengths where this contribution vanishes ("zero-crossings"). At these probe wavelengths, changes in the real part of the index of refraction are small compared to those of the imaginary part, making the heterodyne measurement sensitive to errors in setting the phase of the reference field. We solve this problem with a new balanced detection method that isolates the real part of the signal and is extremely robust against phase errors. The location of the zero-crossings in the population contribution to the index of refraction is found to be complicated by the presence of spectral shifts in the transient absorption that can be characterized and removed with a time-dependent Kramers−Kronig analysis. The spectral shifts are most apparent near the isosbestic points and show similar dynamics to the four-wave mixing signal, suggesting that both are sensitive to the same dynamical processes. These dynamics were observed previously by using four-wave mixing with an off-resonant probe and were assigned to CO migration out of the protein via a number of discrete channels. It appears that both the photoinduced protein conformational relaxation and CO migration through the protein contribute to the transient absorption signal, making the two effects difficult to separate. The direct coupling of the protein motions to the index of refraction changes in the four-wave mixing experiments aids in distinguishing the two processes.

Introduction

Understanding the transport of ligands into and out of proteins is a necessary step toward understanding biological systems. X-ray structures reveal that ligand escape would be impossible if the atoms were confined to thermal fluctuations about their equilibrium positions.[1−3] Clearly, a dynamical pathway must exist that leads to larger correlated motions that permit ligand access to the protein active site. Much recent work has used myoglobin (Mb) as a model system for the study of ligand transport. Techniques of site-specific mutagenesis,[4−7] time-resolved spectrophotometry,[8,9] X-ray crystallography,[10,11] and molecular dynamics simulations[3] have attempted to identify potential escape pathways and characterize the dynamics of ligand escape. Mounting evidence suggests that a few distinct intermediate states exist along the ligand escape pathway. Consistent with this idea, we recently showed that diffractive optics-based heterodyne-detected four-wave mixing spectroscopy reveals volume changes in the protein as it changes conformation to permit ligand escape.[12]

Diffractive-optics based four-wave mixing spectroscopy has been successfully used to study the dynamics of MbCO upon photodissociation and characterize the full range of functionally relevant processes from femtoseconds to milliseconds.[12−15] This technique interferometrically follows protein motions through changes in the real part of the index of refraction (Re $\chi^{(3)}$) that accompany atomic displacements. The very sensitive nature of this observable made it possible to observe the CO escape from Mb in real time.[12] Subsequent transient grating work supports this assignment through the use of high grating wavenumber conditions to further resolve the CO motion.[16] The associated dynamics were found to be well described by a four-barrier model proposed by Beece et al.,[17] and motions along the dynamical pathways between the intermediate states were shown to be related by single activation barriers.

This work exploits the interferometric sensitivity of heterodyne-detected four-wave mixing, or transient grating spectroscopy, to probe protein dynamics. Four-wave mixing signals arise from a number of physical processes, but with care the process of interest can be isolated. In general, the four-wave mixing signal is proportional to the efficiency η with which a probe beam is diffracted from the pump-induced grating:[18−21]

$$\eta \propto |(\Delta n_{\text{protein}} + \Delta n_{\text{Th}} + \Delta n_{\text{ex}}) + i\Delta k_{\text{ex}}|^2 \qquad (1)$$

where $\Delta n_{\text{protein}}$ contains the desired information about the protein dynamics. This term is related to the material strain or the volume change that accompanies protein conformational change.

* Corresponding author: R. J. Dwayne Miller, 80 St. George St., Toronto, ON, M5S 3H6. (416)-978-0354, (416)-978-0366 (fax), dmiller@lphys.chem.utoronto.ca.
† University of Rochester.
‡ University of Toronto.

10.1021/jp014477o CCC: $22.00
Published on Web 09/12/2002

Ideally, one would like to isolate $\Delta n_{protein}$ in biodynamical studies of protein response functions. Contributions to the signal that arise from density changes due to heating, Δn_{Th}, can be removed by performing the studies at the zero-thermal expansion temperature of the protein solution.[12] The terms Δn_{ex} and Δk_{ex} are the electronic contributions of the real and imaginary components of the modulated complex index of refraction, respectively, that arise from the difference in absorption between the MbCO and the photodissociated state. With heterodyne detection, the signal is proportional to $\eta^{1/2}$ and is therefore linear in the refractive index changes. The linearization of the signal permits the separation of real (Re) and imaginary (Im) parts of the signal, such that Δk_{ex} can be easily eliminated. Using an off-resonant probe, Δn_{ex} can be largely reduced.[21,22] However, our previous work using a 1064-nm probe still gave a 16% offset in the signal that we interpreted to be Δn_{ex}. One would like to remove this term completely, since it complicates the isolation of $\Delta n_{protein}$ and provides no new information beyond the transient absorption studies.

The ability to remove Δn_{ex} terms is extremely important for the applications of this spectroscopy to follow energetics and other photodark (nonradiative) processes related to both excited state and reaction dynamics. The protein motions involved in a functional response often involve rms motions of less than 0.1 Å and net volume changes corresponding to changes in effective radius of less than 0.01 Å.[23] The associated energetics driving these processes can be on the order of a single hydrogen bond. These dynamical variables (mass displacement/energetics) are directly related to the biomechanics of protein motion. In this regard, the mechanism by which small amounts of energy can be so efficiently transduced into biological functions such as allosteric regulation is tantamount to understanding the structure−function relationship of biological systems. Information about the minute protein motions and relaxations needs to be correlated to the energetics driving the response. The relatively small changes in the optical properties that accompany these processes require extremely sensitive methods of study. Photothermal, photoacoustic, and four-wave mixing (thermal grating, phase-grating approaches), which enable the study of photodark states, have the requisite sensitivity. They provide a direct measurement of the amount of energy deposited into the sample. Grating spectroscopies are capable of detecting changes in energetics that raise the lattice temperature by less than 10^{-4} °C through changes in density for typical sample conditions. The energy resolution to relaxation processes is more limited by signal-to-noise conditions on the calibration reference. The very small amounts of energy involved in biological processes are detectable within the limits of these techniques (<1 kcal resolution). However, each method has been hampered by either the background spatial modulation of the index of refraction Δn_{ex} or insufficient detector bandwidth in the case of photoacoustic spectroscopy. We show that it is possible to remove Δn_{ex} by tuning the probe wavelength to positions in the absorption difference spectra that yield zero-crossings: wavelengths where $\Delta n_{ex} = 0$. This feature in the Re part of the four-wave mixing signal is analogous to isosbestic points in the absorption difference spectrum.

We begin by outlining an improved diffractive-optics based method for automatic isolation of the Re part of the four-wave mixing signal using differential detection. This method is particularly important for on-resonance four-wave mixing studies where the Im component dominates the signal. In the absence of this approach, small errors in setting the phase of the reference result in poor isolation of the Re part from the large Δk_{ex} component. The four-wave mixing results are then compared to transient absorption data in the Q-band and found to exhibit similar spectral shifts to those reported by Kliger and coworkers.[24] Using singular value decomposition of the transient spectra, we find that the dynamics are similar to those found in the previous four-wave mixing studies,[12] suggesting that the Q-band is also sensitive to ligand motion through the protein. Finally, four-wave mixing data with a tunable probe in the Q-band is presented in order to further verify our assignment of the Δn_{ex} component in the IR studies. At the zero-crossings, the spectral shifts are found to prevent complete isolation of $\Delta n_{protein}$. The effect is relatively minor such that this contribution from Δn_{ex} can be calculated to sufficient accuracy with a time-dependent Kramers−Kronig analysis. The resulting protein contribution and dynamics are fully consistent with the previous IR data. In all cases the dynamics support the concept that CO escapes from the protein via a number of distinct pathways.

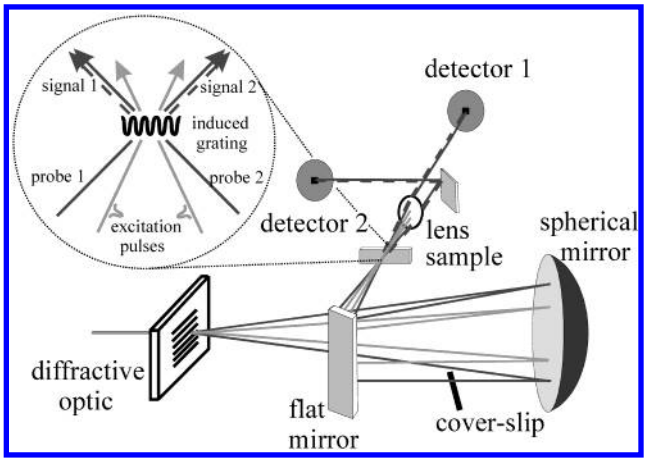

Figure 1. Experimental setup for diffractive optics-based heterodyne-detected four-wave mixing. Diffracted signals are detected at both detectors 1 and 2 and the Re part of the signal is isolated in our balanced detection scheme by taking the difference I_1-I_2. To use the setup with an off-resonant probe, half-wave plates can be inserted into each probe to rotate the polarizations to ±45° with respect to the pump polarization. In this way, the signal from each probe has the same magnitude, and polarizers located before each detector can control the signal/reference ratio to optimize signal-to-noise and heterodyne amplification.[43] The combination of half-wave plates and polarizers was unnecessary for the resonant studies; instead the sample OD was varied to optimize the heterodyne signal.

Materials and Methods

Horse-heart Mb was purchased from Sigma and the MbCO/deoxyMb samples were prepared in Tris buffer as described previously.[15] The sample concentrations were typically ~1 mM to provide an OD of 1. The MbCO/deoxyMb samples were kept under a CO/N_2 environment during the experiment and were flowed through a home-built cell via a peristaltic pump with a flow rate adequate to ensure a new sample for each laser shot. The degree of photolysis was 15% for the transient absorption measurements and approximately 100% for the on-resonance four-wave mixing studies. The high bleach for these experiments was necessary because of the relatively large rms noise of the dye laser that was used as the probe.

The heterodyne-detected four-wave mixing experiment, shown in Figure 1, has been described previously.[12,15,25,26] The current method uses a differential detection scheme for noise reduction[27,28] and to isolate the Real (Re) component of the heterodyne signal. Briefly, a modified Lumonics Sigma 100 was frequency doubled to provide 25-ns excitation pulses at 527

nm and 100-Hz repetition rate. Use of Rhodamine 110 and Rhodamine 6G dyes with a tunable CW dye-laser (Coherent 599) provided probe wavelengths between 550 and 630 nm. The pump and probe beams were incident collinearly upon a diffractive optic (NOI), giving a grating spacing of 3.75 μm at the sample. A mask blocked all but the first-order diffracted beams, which were focused at the sample by a folding and spherical mirror. The diffractive optic ensured that the probe beams were automatically at the Bragg angle for diffraction. The differential detection method required the use of two amplified photodiodes (ThorLabs PDA155), whose output was recorded with a Tektronix TDS520D digitizer.

Our balanced detection technique exploits the symmetry of the setup. The heterodyne signal at detector 1 is given by

$$I_1 = |E_{sig1}|^2 + |E_{ref2}|^2 + 2|E_{sig1}||E_{ref2}| \cos(\phi_{sig1} - \phi_{ref1}) \quad (2)$$

where E_{sig1} is the diffracted signal field from probe 1 and E_{ref2} is the reference field (the undiffracted light from probe 2). This signal can be written explicitly in terms of the Re and Im parts as

$$I_1 = |E_{sig1}|^2 + |E_{ref2}|^2 - 2|E_{ref2}|\{\mathrm{Im}(E_{sig1}) \cos(\phi_1 - \phi_2) + \mathrm{Re}(E_{sig1}) \sin(\phi_1 - \phi_2)\} \quad (3)$$

where ($\phi_1 - \phi_2$) denotes the phase difference between probes 1 and 2. This expression reveals that rotating a coverslip placed in one of the beams can vary the phase difference ($\phi_1 - \phi_2$) to isolate the Re and Im components of the signal.[15] This procedure, however, requires some knowledge of either the Re or Im parts to correctly assign the different signal components. In the past, we identified the Im part by matching it to the transient absorption signal and then used a coverslip calibrated for a 90° phase shift to recover the Re part of the signal. We have also used purely real thermal or acoustic signatures for the phase calibration.

This approach is limited to cases where the signal of interest (we will assume this is the Re part) is comparable to or larger than the Im part, as was the case in the previous off-resonance studies. In this case, with phase errors of ±10°, the signal contamination by the Im part would be 3% or less. However, this phase tolerance is greatly reduced if $\mathrm{Re}(\chi^{(3)}) \ll \mathrm{Im}(\chi^{(3)})$, as happens for resonant probes near zero-crossings in the Δn_{ex} term. In this case, a new procedure is needed to reduce the sensitivity of the signal response to the absolute phase setting. By exploiting the symmetry of the four-wave mixing beam geometry, this condition can be realized. The new detection scheme demonstrated in this work is relatively straightforward.

The symmetry of the setup reveals that the signal at detector 2 can be written as

$$I_2 = |E_{sig2}|^2 + |E_{ref1}|^2 - 2|E_{ref1}|\{\mathrm{Im}(E_{sig2}) \cos(\phi_2 - \phi_1) + \mathrm{Re}(E_{sig2}) \sin(\phi_2 - \phi_1)\} \quad (4)$$

Inspection of eq 3 readily demonstrates that the difference in the signals at detectors 1 and 2 can be used to isolate the Re component of the signal, provided the amplitudes of the signal and reference field are equal; i.e.,

$$I_1 - I_2 = 4|E_{ref2}|\mathrm{Re}(E_{sig1}) \sin(\phi_2 - \phi_1) \quad (5)$$

This result arises from the use of the diffractive optic and its inherent symmetry in the thin diffraction limit. The ±1 orders are equal amplitude and symmetrically located about the normal to the diffractive optic. Thus, the field that provides the probe at one detector provides the reference at the other. By differential detection of I_1 and I_2, it is possible to isolate the Re part of the signal with a high degree of immunity to errors in the phase setting. This feature is shown in Figure 2 where changes in the phase setting from the optimal position of up to 75° still gave Re signals that agreed to within 3%. The only change was a reduction of the signal amplitude, but even this was tolerable. This new detection protocol reduces the sensitivity of the method to errors in the phase setting by at least an order of magnitude. This was an essential development for the visible probe experiments for wavelengths where the Im component of the signal was significantly larger than the Re part. The method also provided important information about the relative phases of signal and reference. For example, when the difference signal was zero, this indicated that the phase difference was set to the Im part ($\phi_2 - \phi_1 = 0$), whereas when the difference was maximized, it was set to the Re part ($\phi_2 - \phi_1 = \pi/2$). The method also improved the signal-to-noise by subtracting the laser noise associated with the reference field.[27,28]

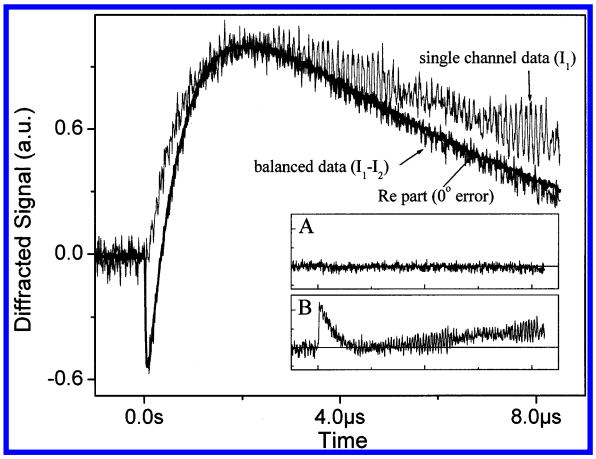

Figure 2. Room-temperature four-wave mixing signals for MbCO (probe 1064 nm grating spacing 7.5 μm), illustrating the effectiveness of the balanced detection method. For a phase error of 75°, use of balanced detection (I_1-I_2) maintains the form of the 0° phase error signal, though the signal amplitude is greatly decreased. The data shown have been normalized for comparison purposes. Single channel detection (I_1) shows large deviations in the form of the signal, as well as poor signal-to-noise as a result of laser noise that is automatically subtracted in the balanced detection scheme. Inset A shows the residual difference between the normalized balanced data at 75° phase error and the 0° data. Inset B shows much larger difference between the single channel detection (also at 75° phase error) and the 0° data.

For the transient absorption experiments the DOE was removed, leaving the pump and probe collinear at the sample. As in the four-wave mixing experiment, the probe polarization was set to the magic angle with respect to the pump to prevent anisotropic effects and rotational diffusion from complicating the dynamics. The beams were separated with a prism before detecting the probe transmission at a single detector recorded over a wavelength range of 550−630 nm at 0.5 nm intervals.

Results and Discussion

I. Transient Absorption in the Q-Band. As noted in our previous work,[12] there is a relatively large change in index of refraction $\mathrm{Re}(\chi^{(3)})$ that accompanies ligand motion through the protein and escape out of the protein. The change is significant enough to consider closer inspection of the changes in transient absorption spectra. Furthermore, as discussed above, it would be desirable to remove the contributions to the modulated index of refraction from excited state or population terms. This goal

can be achieved at zero-crossings in the index of refraction terms due to changes in the sample's absorption. For both of these reasons, it is important to characterize the transient absorption spectrum. It has been established that the transient absorption spectrum completes the majority of its evolution toward the equilibrium difference spectrum between MbCO and DeoxyMb within 30 ps[29] for aqueous solutions near physiological conditions. However, the structural changes of the protein clearly occur on much longer time scales. The coupling of the protein relaxation will be strongest for motions near the heme and strongly attenuated for more remote displacements. Since the CO motion through the protein undoubtedly involves displacements away from the heme site, these structural changes will only manifest themselves as secondary effects to the initial relaxation in the heme vicinity following ligand photodissociation. Small spectral shifts are the primary observable and these are most sensitively detected at the isosbestic points in the equilibrium difference spectrum of MbCO and deoxyMb. The magnitude of these shifts needs to be characterized and incorporated into the transient absorption spectrum to correctly identify the zero-crossings in the population contribution to the index of refraction in the four-wave mixing studies to be discussed below.

Several transient absorption studies have revealled long-lasting spectral shifts in MbCO. In a footnote, Henry et al.[30] suggested the possibility of Soret band spectral shifts that were distinct from geminate rebinding lasting for nanoseconds in aqueous solution. Upon closer examination it was concluded that the dynamics yielding the dominant spectral shifts were completed within the first 30 ps.[29] Many subsequent studies used glycerol/water solvents, which does not permit direct comparison with our results in aqueous solution. Several of these studies focused on band III and found that it exhibited a shift of the full band assigned to the displacements of the iron out of the porphyrin ring plane[31] and was a highly stretched exponential process lasting as long as microseconds.[8] Other glycerol/water studies by Lambright et al.[4,32] report Soret band shifts indicating dynamics on the microsecond time scale that they attribute to ligand rebinding or conformational changes associated with ligand escape from the protein. In these studies the protein relaxation and associated ligand transport out of the protein are strongly damped or "slaved" to the surrounding highly viscous glycerol/water solvent. More relevant to this work, Ansari et al.[33] showed that there are small Soret band shifts lasting as long as microseconds in aqueous solution at room temperature. Kliger and co-workers have more recently reported spectral shifts in the Q-band,[24] where they observed a 400-ns process at room temperature in aqueous solution, which they attributed to migration of water into the heme pocket or conformational changes associated with ligand escape.

Specifically, the spectral shifts on the nanosecond time scale should be composed of two nearly independent relaxation coordinates: a relaxation process that accompanies ligand dissociation, and another that involves CO migration through the protein. In the latter case, protein thermal fluctuations are required for the CO to sample other regions in the surrounding globin. Since the volume occupied by the CO is larger than the void spaces in the protein, the movement of the CO away from the heme pocket should also lead to a spectral shift, albeit a secondary effect as discussed above. The higher sensitivity of the Re term in the four-wave mixing signal to the CO motion enables the CO dynamics to be identified. In the interest of furthering our recent study of CO escape, and to make a connection to previous transient absorption studies, it was worth reexamining the exact functional form and spectral dependence of these shifts.

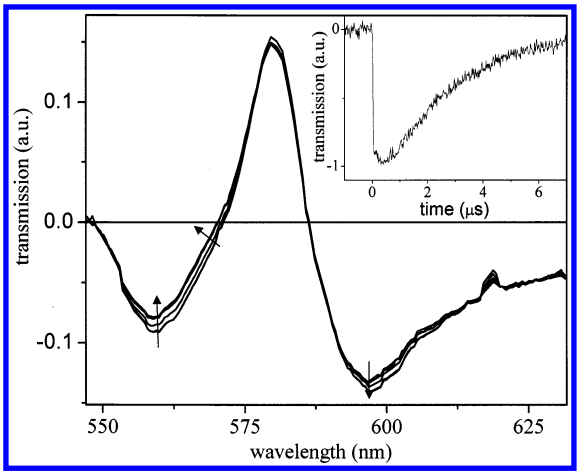

Figure 3. Transient absorption in the Q-band. Wavelength spectrum at −1.5 °C at 100 ns, 500 ns, 2 μs, 5 μs, and 7.5 μs after photodissociation (arrows indicate time progression). The inset shows the time-resolved signal at 570.5 nm, close to the isosbestic point, where the amplitude of the spectral shift is the largest and the most sensitive to structural changes.

The transient absorption spectrum from 550 to 630 nm at −1.5 °C (where Δn_{Th} is negligible in the grating signal[12]) is shown in Figure 3, exhibiting time-dependent regions of increasing and decreasing intensity at 570 and 600 nm, respectively. The overall integrated intensity remains constant to within 1%. At 570 nm the magnitude of the shift is ∼30 cm^{-1}. We analyzed the time-resolved signal at different wavelengths by singular value decomposition (SVD),[34,35] to obtain time-dependent eigenvectors and wavelength-dependent amplitudes, shown in Figure 4. The eigenvectors were fit with multiple exponential decays by a Levenberg−Marquardt algorithm.[34]

At both temperatures, the SVD analysis gave two dominant eigenvalues, with additional smaller components improving the χ^2 fit by less than 5 x 10^{-3}. Component I, shown in the top left corner, matches the equilibrium difference spectrum (MbCO-deoxyMb, see Figure 3) and can therefore be assigned to dissociation/recombination, while component II has very different features, indicating that it arises from a distinct process. The time dependence in component I is very small, confirming that the rebinding is negligible on the time scale of our experiments (25 ns−8 μs).[33] Component II describes the spectral shifts that exhibit two characteristic time decays, with amplitudes and decay rates listed in Table 1. For comparison, processes extracted from the four-wave mixing studies that describe CO motions inside the protein[12] are also given, using the previous nomenclature for the dynamics associated with different CO sites within the protein (vide infra). The amplitude ratio A_1/A_2 is reported here at −1.5 °C, where the protein component of the signal is readily observed and process 1 is no longer as close to the limit of our time resolution (25 ns).The amplitude ratio for the transient absorption data was found to be −0.36 but is not listed in Table 1 because it is not directly comparable to the four-wave mixing amplitudes, which depend on the volume changes associated with the C → D and D → S transitions.

It is noted here that the specific functional form of the spectral shifts may be fit to stretched exponential terms usually attributed to glasslike relaxation dynamics.[8,36] However, the spectral shifts and transient absorption data contain terms from both protein relaxation following ligand dissociation and ligand transport effects. The two coordinates are related to fluctuation and

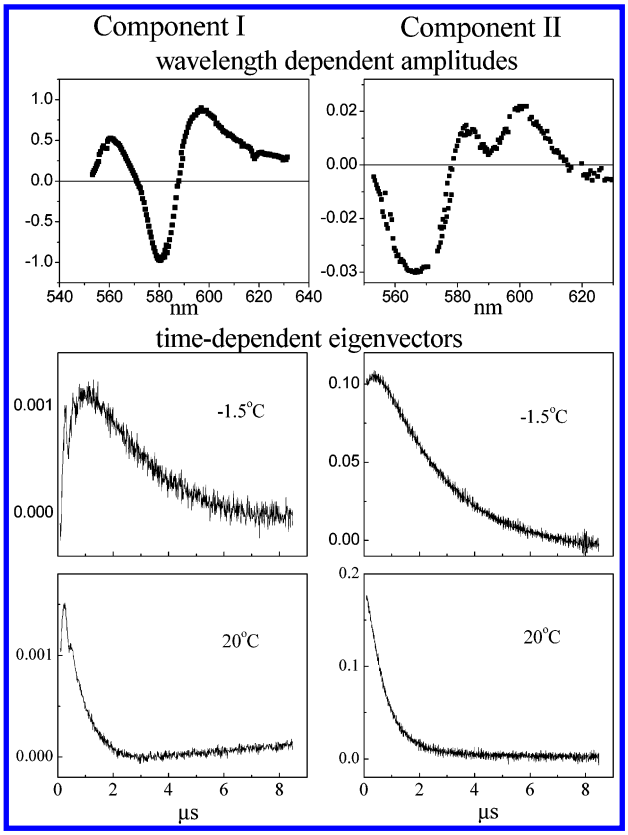

Figure 4. Wavelength and time-dependent amplitudes from the SVD analysis. The left column pertains to component I, which we assign to photolysis and rebinding. Component II, shown on the right, represents a process distinct from geminate rebinding.

dissipation processes at different regions in the protein and therefore should exhibit different dynamics. As seen from Table 1, the close agreement with the previous off-resonant grating studies that were found to be sensitive to CO transport[12] and escape from the protein[12,16] suggest that the spectral shifts are also largely determined by perturbations in the protein structure associated with CO migration through the protein. There is, however, a difference in that the effect of the CO motion through the protein is only manifest as a secondary effect in the Im term (i.e., spectral shifts), whereas the Re term (off-resonance) is largely dominated by the effect of the mass displacements or protein volume (strain) changes.

The reported dynamics in Table 1 can be taken to be in reasonable agreement with the previous work by Kliger and co-workers who also report nanosecond spectral shifts on the order of a few nanometers.[24] They find a 400-ns process at room temperature that they attribute to either ligand motion or the movement of water into the protein. The decay measured in this earlier study (room temperature only) could be a combination of the two processes found in the present study, i.e., a combination of the 67 and 685 ns components. The absence of a fast component can be attributed to their limited sampling in time. In addition, the discrepancy between the observed decay rates may be due to the different spectral bandwidths of the two methods: a Xe arc lamp based spectrometer in combination with a 15 point Savitzky-Golay smoothing operation of their 500−650-nm data (sampled at 250 wavelengths) before the SVD analysis[24] would include a much larger bandwidth than the present transient absorption data collected from a dye laser probe (∼0.5 Å bandwidth). We verified this point by repeating our SVD analysis after averaging our absorption data to include a bandwidth of 2 nm. We found that the slower decay component did in fact decrease the decay rate by ∼100 ns, bringing it closer to the value obtained by Esquerra et al.[24] Our single-wavelength transient absorption data are also well-described by a two-exponential fit (recall that the bimolecular rebinding is negligible on the time scale of this experiment). The two components had decays of 118 ± 33 ns and 650 ± 90 ns at room temperature and 418 ± 22 ns and 2.2 ± 0.3 μs at −1.5 °C temperature, in good agreement with the SVD analysis. The magnitude of the spectral shifts we observe at 570 nm is 30 cm^{-1}, which is consistent with Soret band shifts reported by Ansari et al.[33] The similarities between τ_1 and τ_2 in the two distinct experiments is striking and make the assignment of the origin of the spectral shifts in this manner straightforward. The spectral shifts imply that the Q-band is sensitive to structural reorganization following the CO motions inside the protein, more precisely the CO moving among the Xenon sites before escaping to the solvent.[37,38]

In a previous study[12] we described the observed dynamics in terms of a four-barrier model for ligand escape:[17]

$$A \leftrightarrow B \leftrightarrow C \leftrightarrow D \leftrightarrow S$$

where A is the bound state, B is where the CO is unbound but still in the heme pocket, C and D represent the state where CO is in two intermediate cavities, and S is after the CO has escaped to the solvent. The combination of our time resolution (∼25 ns) and the fact that we use aqueous solvent means that we do not resolve the B state, prohibiting us from distinguishing between the four-barrier and the three-barrier model used by other groups. To relate the observed dynamics to the four-barrier model we note that the processes reported in Table 1 are well separated in time and employ the steady-state approximation.[4,7,30] The detailed relations are given in the Supplementary Information accompanying the work of Franzen[7] and allow us to assign the exponential processes characterized by τ_1 and τ_2 to the C → D and D → S transitions. A separate argument, independent of the kinetic model used, can identify the τ_2 process as the ligand escape: the large volume change associated with the CO solvation is directly evident in the transient grating signal[12,16] and provides a distinct signature for the CO escape.

There have been a number of kinetic models used to describe post-photolysis dynamics observed through spectral shifts and other observables. Table 2 is not an exhaustive list, but serves to illustrate the variety of models used and the variation in their results. In particular we restrict the list to studies done under similar solvent conditions or studies that include modeling of solvent effects. We focus on the ligand escape time as determined by the different models and techniques. The evidence in the literature for this effect in terms of kinetics is not completely consistent but trends are evident. Each method supports the involvement of various intermediates along the CO escape pathway, with the number of intermediates being a function of solvent and temperature conditions, as well as instrument sensitivity. The most commonly used models are sequential, an idea that is supported by recent X-ray studies of Srajer et al.[10] Alternately, the recent site-specific mutagenesis work of Scott et al.[6] strongly suggests the use of a side-path model. It is interesting to note that the Soret band transient absorption studies of Lambright et al.[4] and Ansari et al.[33] report similar exponential components in glycerol/water, but their different models lead to different estimates of ligand escape time. This difference likely arises from the difficulty in modeling the combination of conformational relaxation and geminate rebinding in transient absorption data. Many glycerol/water studies[4,7,8] show stretched exponential behavior for the initial

TABLE 1: Biexponential Fitting Parameters to Transient Absorption and Four-Wave Mixing Data (Not Including Bimolecular Recombination)[a]

	$T = 20$ °C		$T = -1.5$ °C		
experimental method	τ_1 ($\sim\tau_{CD}$)	τ_2($\sim\tau_{DS}$)	τ_1 ($\sim\tau_{CD}$)	τ_2 ($\sim\tau_{DS}$)	A_1/A_2*
transient absorption component II	67 ± 19 ns	685 ± 7 ns	439 ± 26 ns	2340 ± 37 ns	
4-wave mixing (Re part of the signal), 1064 nm probe[12]	50 ± 20 ns	725 ± 20 ns	220 ± 70 ns	2860 ± 20 ns	−0.14
4-wave mixing (Re part of the signal), 579 nm probe			193 ± 13 ns	2859 ± 18 ns	−0.41

[a] Note that the amplitudes for process 1 are negative in all cases.

TABLE 2: Summary of Various Kinetic Models and Their Results for CO Ligand Escape Times

authors (method)	model (where stated)	medium (protein)	T, °C	τ_{escape}	H_{DS}, kJ/mol
Dadusc et al.[12] (4-wave mixing)	A ↔ B ↔ C ↔ D ↔ S	water (horse-heart Mb)	20	$\tau_{DS} = 725 \pm 15$ ns	31 ± 1,[a] 42 ± 1[b]
			−1.5	$\tau_{DS} = 2860 \pm 20$ ns	
(Q-band transient absorption−present work)			20	$\tau_{DS} = 685 \pm 7$ ns	
			−1.5	$\tau_{DS} = 2340 \pm 37$ ns	
Sakakura et al.[16] (4-wave mixing and photoacoustic spectroscopy)	A ↔ B ↔ C ↔ S	water (sperm-whale Mb)	20	$\tau_{CS} = 700$ ns	42 ± 1
			0	$\tau_{CS} = 2800$ ns[c]	
Jackson et al.[41] (IR transient absorption)	B, C intermediates obsd	water (horse skeletal muscle)	10	~1 μs	
Srajer et al.[10] (time-resolved X-ray diffraction)	2 intermediates obsd	crystal (sperm-whale Mb)	20	~10 μs	
Esquerra et al.[24] (Q-band transient absorption)	biexponential fit	water (horse skeletal muscle)	20	$\tau_1 = 370 \pm 30$ ns[d]	
Beece et al.[17] (flash photolysis)	A ↔ B ↔ C ↔ D ↔ S	water (sperm-whale Mb)	20	$\tau_{DS} = 420$ ns[e]	36
			−1.5	$\tau_{DS} = 1900$ ns[e]	
Henry et al. [30] (Soret band transient absorption)	A ↔ B ↔ S	water (sperm-whale Mb)	20	$\tau_{BS} = 190 \pm 30$ ns	
Scott et al.[6] (flash photolysis) (O_2 ligand)	A ↕ C↔B↔S	water (sperm-whale Mb)	20	$\tau_{BS} = 160 \pm 25$ ns	
Franzen[7] (Soret band transient absorption)	A ↔ B ↔ S	water (H93G mutants)	20	$\tau_{BS} = 460$ ns[f]	44

[a] Calculated by using viscosity-dependent Kramers eq 10 of Beece et al.[17] [b] Calculated by using Arrhenius law (no viscosity dependence). [c] Estimated from Figure 10 of ref 16. [d] Esquerra et al.[24] assign this exponential component to ligand escape or water migration. [e] Rates adjusted for appropriate viscosity and temperature using the model of Beece et al. (factor of 2 error bar reported).[17] [f] Averaged over four different proximal adducts of H93G mutant.

dynamics, and Tian et al.[39] find a geminate phase that can be fit by a stretched exponential with $\beta = 0.5$ in aqueous solution at 293 K. This latter work was primarily concerned with the relaxation dynamics of the "open" and "closed" conformational states of myoglobin as probed by pH dependence and may be important in ligand escape. In a previous paper[12] we showed that our data could not be fit with a stretched exponential function. We note that the four-wave mixing and Q-band transient absorption results we report in this paper give ligand escape times that are within the range of values in Table 2. We find a ligand escape barrier of 31 kJ/mol based on the Kramers treatment of Beece et al.,[17] which compares favorably with their value of 36 kJ/mol. As the limited temperature range of our measurement (21.5 °C) prevents us from distinguishing between Arrhenius and Kramers behavior, we also report a barrier of 42 kJ/mol determined from the Arrhenius law. This value agrees well with Sakakura et al.[16] and Franzen,[7] as well as recent work of Cao et al.,[40] who measure 42 kJ/mol for H_2O binding and CO escape from ferrous Mb using an Arrhenius treatment.

Of the methods listed here, X-ray diffraction, IR spectroscopy, and four-wave mixing are better suited to measure ligand escape than others because they are directly sensitive to the CO ligand. X-ray diffraction probably gives the best picture of the ligand escape process because it structurally resolves the intermediate states. Srajer et al.[10] report two docking sites of the photodissociated CO. At room temperature the first of these has a half-life for decay of ~100 ns and the other of several microseconds, in reasonable agreement with the transient absorption and four-wave mixing data we present here (note that Sakakura et al.[16] do not resolve the faster component, possibly because they do not use heterodyne detection, which improves signal-to-noise and allows better identification of the different signal components). The IR studies of Jackson et al.[41] resolve an intermediate state that decays with a time constant of a few hundred nanoseconds at room temperature, consistent with our findings.

The data given in Table 2 and the agreement between the transient absorption and four-wave mixing data in Table 1 suggest that, although they have varying degrees of sensitivity to the CO motion, both methods provide a picture of the dynamics along the ligand migration pathway. We now use these methods in concert to examine the electronic contribution, Δn_{ex}, to the four-wave mixing signal. This contribution is large for the resonant-probe four-wave mixing experiments but can be removed through location of the time-dependent zero-crossings in the index of refraction.

II. Removing the Δn_{ex} Contribution to the Four-Wave Mixing Signal. The Kramers−Kronig relations[42] dictate that spectral shifts will be accompanied by a time-dependent Δn_{ex}. The motivation for using a resonant probe for the four-wave mixing studies was to remove Δn_{ex} by tuning the probe to a zero-crossing as discussed. Clearly, this can only work if the position of the zero-crossing remains fixed in time. To investigate the effect of the spectral shifts on the time dependence of Δn_{ex}, a time-dependent Kramers−Kronig calculation was performed, using the Kramers-Kronig relation:

$$\Delta n_{ex}(\omega,t) = \frac{c}{2\pi} P \int_{-\infty}^{\infty} \frac{\Delta\alpha(\omega',t)}{\omega'(\omega' - \omega)} d\omega' \qquad (6)$$

where P refers to the Cauchy principal value, c is the speed of light, and ω is the frequency of radiation. The optical density is given by $\Delta\alpha(\omega) = 4\pi d\Delta k_{ex}/(2.3\lambda)$[18] where d is the sample thickness. The Kramers−Kronig calculation of Δn_{ex} from the equilibrium difference spectrum of MbCO and deoxyMb is

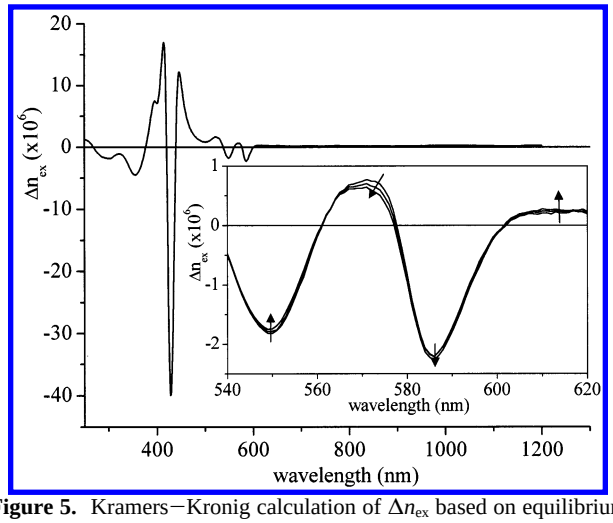

Figure 5. Kramers−Kronig calculation of Δn_{ex} based on equilibrium absorption spectra at −15 °C. The equilibrium data were used in combination with the time-dependent Q-band transient absorption data to compute the time dependence of Δn_{ex} within the Q-band. The time-dependent data are shown in the inset for times 100 ns, 2 μs, and 7.5 μs.

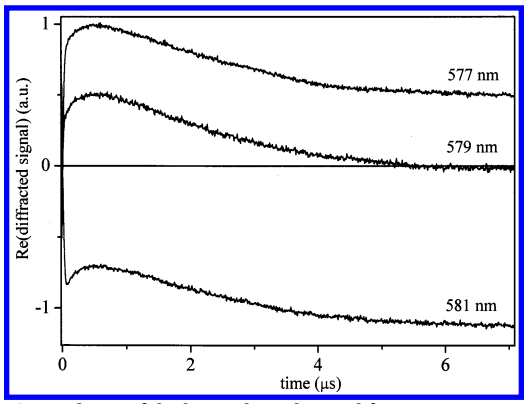

Figure 6. Real part of the heterodyne-detected four-wave mixing signal for MbCO at −1.5 °C for wavelengths near the zero-crossings in Δn_{ex} at 579 nm.

shown in Figure 5. To calculate the time dependence of Δn_{ex}, caused by the Q-band spectral shifts, the time dependent 550 nm−630 nm portion of the spectrum (shown in Figure 1) was spliced into the equilibrium difference spectrum. The integration was performed with spectra at time intervals of 25 ns and the results were interpolated to determine the full $\Delta n_{ex}(t)$. Although the full time-dependent spectrum was not available for this analysis, Kramers−Kronig calculations show that the Q-band is reasonably well-isolated: simulations of spectral shifts of 1 nm in the Soret band affected the computed $\Delta n_{ex}(t)$ in the Q-band by less than 10%. This is a reasonable assumption, since the most significant spectral shifts in the Soret and band III are reported to occur within the first 30 ps,[29] and nanosecond spectral shifts in the Soret band as reported by Ansari et al.[33] are smaller than 1 nm in aqueous solution at −2 °C.

The inset of Figure 5 illustrates Δn_{ex} at several time delays to indicate the time dependence. It is clear that the Q-band spectral shifts cause a significant time-dependence in Δn_{ex} near 579 nm but have little effect off-resonance. This is expected as the dispersion in $\Delta n_{ex}(\partial \Delta n_{ex}/\partial \lambda)$ is changing most rapidly near the zero-crossings. Further, the effect of spectral shifts was anticipated to be negligible as the index of refraction changes far from resonance are largely dominated by the magnitude of the absorption changes in the Soret region and should be relatively immune to second-order effects involving Q-band

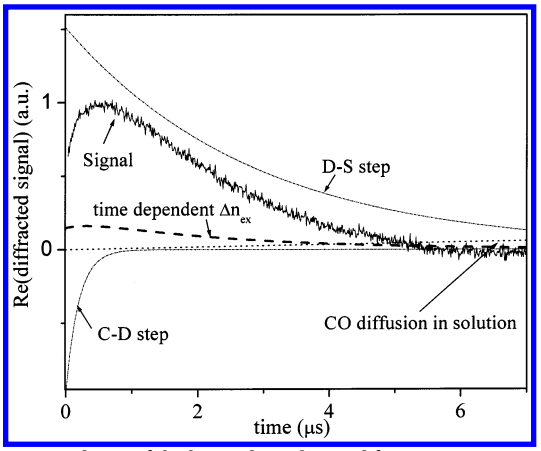

Figure 7. Real part of the heterodyne-detected four-wave mixing signal for MbCO at −1.5 °C for wavelengths at 579 nm. The separated contributions to the signals are shown: Δn_{ex}, protein contributions k_{CD} and k_{DS}, and CO diffusion in the solution.[12]

spectral shifts. This analysis confirms this point. The dynamics associated with CO motion through the protein are far more distinctive at lower temperatures. Figure 6 shows the Re part of the heterodyne signal at −1.5 °C for different probe wavelengths close to the zero-crossing at 579 nm. Note that these signals have not been normalized for laser power, detector sensitivity, and absorption differences at the different wavelengths and are meant to show qualitative trends only. From the IR studies we found that the CO had escaped and the protein was fully relaxed by ∼7 μs.[12] The offset in the signal at 7 μs was believed to be Δn_{ex}. The present experiment supports this interpretation: at 7 μs, the offset crosses zero within 1 nm of the expected crossing as predicted by the Kramers−Kronig relations. Moreover, the calculation shows that Δn_{ex} changes by <1% with these spectral shifts taken into account at our previous probe wavelength of 1064 nm. The assignment of the offset to Δn_{ex} at this time scale and this wavelength is then fully justified.

To completely isolate $\Delta n_{protein}$, the residual Δn_{ex} was first calculated from the time-dependent Kramers−Kronig and then subtracted. This was done by comparing the relative magnitudes of the signal components with the IR probe to determine the magnitude of the Δn_{ex} signal. It was found to be 15% of the total amplitude at $t = 0$. The parameters related to $\Delta n_{protein}$ measured at 579 nm are summarized in Table 1, and the different components of the measured signal are shown in Figure 7. The ratio of the amplitudes are quite different at the two wavelengths. This discrepancy may be explained by the fact that the experiment was done at the magic angle at 579 nm but not at 1064 nm. Although the anisotropy was included in the modeling of the 1064-nm data, it had an amplitude opposite to the C→D process and occurred on a similar time scale and may not have been completely removed. As expected, the decay times for the C→D and D→S processes agree very well at both 579 and 1064 nm.

In summary, we have investigated the dynamics of MbCO on the nanosecond time scale by Q-band transient absorption and resonant four-wave mixing. The transient absorption dynamics we observed are consistent with other work.[4,24,32,33] The similarity between the dynamics of the Q-band transient absorption and previous transient grating studies suggests that the transient absorption dynamics (25 ns $\leq t \leq$ 8 μs) arise predominantly from conformational change that accompanies ligand escape. We demonstrated a new balanced detection method that is particularly useful for resonant four-wave mixing

studies where $\mathrm{Re}(\chi^{(3)}) \ll \mathrm{Im}(\chi^{(3)})$. The method provides automatic separation of the Re part of the signal and greatly reduces the sensitivity of heterodyne detection to phase setting errors. Although isolation of the protein contribution to the four-wave mixing signal was complicated by the spectral shifts in the Q-band, the time-dependent Kramers−Kronig analysis allowed us to remove the effect. The present on-resonance results were found to be in good agreement with our earlier off-resonance work.[12] Both studies are consistent with CO escape through a well-defined path or discrete set of pathways. The time scale measured for CO escape is also consistent with work listed in Table 2. The effect of ligand motion through the protein is more sensitively detected using off-resonance probes; however, the electronic contribution will always represent a small contribution that is difficult to define. This contribution needs to be determined independently or eliminated from the signal in studies involving very small effects such as protein conformational changes. We have demonstrated a general method of achieving this separation by tuning the probe wavelength to the zero-crossings to eliminate Δn_{ex} and facilitate the assignment of the components of the four-wave mixing signal to specific dynamical processes. This general method should have numerous applications in the study of photochemical processes that require information about nonradiative channels and energetics, as well as population dynamics. This approach will be particularly useful in the study of biological problems, where these same issues also involve minute atomic displacements that are part of the protein function and are central in the structure/function relationship.

Finally, the connection of the present study to CO transport out of the protein demonstrates the sensitivity of the method and provides further insight into a fundamental issue relevant to protein function. The observed dynamics are consistent with earlier off-resonance four-wave mixing studies that demonstrated that the CO escape from the protein involves distinct intermediates. The intermediate states have been attributed to CO sampling of voids within the protein structure that have been identified through X-ray diffraction studies[10,11] of Xe binding sites. These voids are thought to be integral to assisting ligand transport in and out of the protein. The discrete nature of the CO transport process revealed both in crystals through time-resolved X-ray diffraction studies,[10] IR spectroscopy,[41] these[12] and related grating studies,[16] and transient absorption methods[4,6,7,24,33] indicates that ligand transport to and from active sites is encoded in the protein structure. Dynamics are central to the overall mechanism as there are significant barriers to ligand transport. Protein fluctuation and conformational sampling must create passageways with sufficient correlation lengths for the ligand to permit access to built-in void spaces within the protein.[12,23]

Acknowledgment. This work was supported by the Natural Science and Engineering Research Council of Canada.

References and Notes

(1) Nobbs, C. L. *Hemes and Hemeproteins*; Academic Press: New York, 1966.
(2) Case, D. A.; Karplus, M. *J. Mol. Biol.* **1979**, *132*, 343.
(3) Elber, R.; Karplus, M. *J. Am. Chem. Soc.* **1990**, *112*, 9161.
(4) Lambright, D. G.; Balasubramanian, S.; Boxer, S. G. *Biochemistry* **1993**, *32*, 10 116.
(5) Scott, E. E.; Gibson, Q. H. *Biochemistry* **1997**, *36*, 11 909.
(6) Scott, E. E.; Gibson, Q. H.; Olson, J. S. *J. Biol. Chem.* **2001**, *276*, 5177.
(7) Franzen, S. *J. Phys. Chem. B* **2002**, *106*, 4533.
(8) Jackson, T. A.; Lim, M.; Anfinrud, P. A. *Chemical Physics* **1994**, *180*, 131.
(9) Lim, M.; Jackson, T. A.; Anfinrud, P. A. *Science* **1995**, *269*, 962.
(10) Srajer, V.; Ren, Z.; Teng, T.-Y.; Schmidt, M.; Ursby, T.; Bourgeois, D.; Pradervand, C.; Schildkamp, W.; Wulff, M.; Moffat, K. *Biochemistry* **2001**, *40*, 13 802.
(11) Chu, K.; Vojtchovsky, J.; McMahon, B. H.; Sweet, R. M.; Berendzen, J.; Schlichting, I. *Nature* **2000**, *403*, 921.
(12) Dadusc, G.; Ogilvie, J. P.; Schulenberg, P.; Marvet, U.; Miller, R. J. D. *Proc. Natl. Acad. Sci.* U. S. A. **2001**, *98*, 6116.
(13) Goodno, G. D.; Astinov, V.; Miller, R. J. D. *J. Phys. Chem. A* **1999**, *103*, 10630.
(14) Goodno, G. D.; Astinov, V.; Miller, R. J. D. *J. Phys. Chem. A* **1999**, *103*, 10619.
(15) Dadusc, G.; Goodno, G. D.; Chiu, H. L.; Ogilvie, J. P.; Miller, R. J. D. *Isr. J. Chem.* **1998**, *38*, 191.
(16) Sakakura, M.; Morishima, I.; Terazima, M. *J. Phys. Chem. B* **2001**, *105*, 10424.
(17) Beece, D.; Eisenstein, L.; Frauenfelder, H.; Good, D.; Marden, M. C.; Reinisch, M. L.; Reynolds, A. H.; Sorensen, L. B.; Yue, K. T. *Biochemistry* **1980**, *19*, 5147.
(18) Nelson, K. A.; Casalegno, R.; Miller, R. J. D.; Fayer, M. D. *J. Chem. Phys.* **1982**, *77*, 1144.
(19) Miller, R. J. D. *Time-Resolved Spectroscopy*; Wiley & Sons: New York, 1989.
(20) Richard, L.; Genberg, L.; Deak, J.; Chiu, H. L.; R. J. D, M. *Biochem.* **1992**, *31*, 10 703.
(21) Deak, J.; Richard, L.; Periera, M.; Chui, H. L.; Miller, R. J. D. *Methods Enzymol.* **1994**, *232*, 322.
(22) Deak, J.; Chiu, H. L.; Lewis, C. M.; Miller, R. J. D. *J. Phys. Chem. B* **1998**, *102*, 6621.
(23) Miller, R. J. D. *Acc. Chem. Res.* **1994**, *27*, 145.
(24) Esquerra, R. M.; Goldbeck, R. A.; Kim-Shapiro, D. B.; Kliger, D. S. *Biochemistry* **1998**, *37*, 17527.
(25) Goodno, G. D.; Dadusc, G.; Miller, R. J. D. *J. Opt. Soc. Am. B* **1998**, *15*, 1791.
(26) Goodno, G. D.; Astinov, V.; Miller, R. J. D. *J. Phys. Chem. B* **1999**, *103*, 603.
(27) Abbas, G. L.; Chan, V. W. S.; Yee, T. K. *J. Lightwave Technol.* **1985**, *LT-3*, 1110.
(28) Yuen, H. P.; Chan, V. W. S. *Opt. Lett.* **1983**, *8*, 177.
(29) Janes, S. M.; Dalickas, G. A.; Eaton, W. A.; Hochstrasser, R. M. *Biophys. J.* **1988**, *54*, 545.
(30) Henry, E. R.; Sommer, J. H.; Hofrichter, J.; Eaton, W. A. *J. Mol. Biol.* **1983**, *166*, 443.
(31) Srajer, V.; Champion, P. M. *Biochemistry* **1991**, *30*, 7390.
(32) Lambright, D. G.; Balasubramanian, S.; Boxer, S. G. *Chem. Phys.* **1991**, *158*, 249.
(33) Ansari, A.; Jones, C. M.; Henry, E. R.; Hofrichter, J.; Eaton, W. A. *Biochemistry* **1994**, *33*, 5128.
(34) Press, W. H.; Teukolsky, S. A.; Vetterling, W. T.; Flannery, B. P. *Numerical Recipes in C*, 2nd Ed.; Cambridge University Press: New York, 1992.
(35) Henry, E. R.; Hofrichter, J. *Methods Enzymol.* **1992**, *210*, 129.
(36) Scher, H.; Shlesinger, M. F.; Bendler, J. T. *Phys. Today* **1991**, *44*, 26.
(37) Tilton, R. F.; Kuntz, I. D., Jr.; Petsko, G. A. *Biochemistry* **1984**, *23*, 2849.
(38) Frauenfelder, H.; McMahon, B. H.; Austin, R. H.; Chu, K.; Groves, J. T. *Proc. Nat. Acad. Sci. U. S. A.* **2001**, *98*, 2370.
(39) Tian, W. D.; Sage, J. T.; Champion, P. M.; Chien, E.; Sligar, S. G. *Biochemistry* **1996**, *35*, 3487.
(40) Cao, W.; Christian, J. F.; Champion, P. M.; Rosca, F.; Sage, T. *Biochemistry* **2001**, *40*, 5728.
(41) Jackson, T. A.; Lim, M.; Anfinrud, P. A. *Int. Conf. Time-Resolved Vib. Spectrosc., 7th* **1995**, 9.
(42) Saleh, B. E. A.; Teich, M. C. *Fundamentals of Photonics*; John Wiley and Sons: New York, 1991.
(43) Levenson, M. D.; Eesley, G. L. *Appl. Phys.* **1979**, *19*, 1.